



**HAL**  
open science

# Repurposing a Bio-Inspired NiFe Hydrogenase Model for CO<sub>2</sub> Reduction with Selective Production of Methane as the Unique C-Based Product

Md Estak Ahmed, Suzanne Adam, Dibyajyoti Saha, Jennifer Fize, Vincent Artero, Abhishek Dey, Carole Duboc

► **To cite this version:**

Md Estak Ahmed, Suzanne Adam, Dibyajyoti Saha, Jennifer Fize, Vincent Artero, et al.. Repurposing a Bio-Inspired NiFe Hydrogenase Model for CO<sub>2</sub> Reduction with Selective Production of Methane as the Unique C-Based Product. ACS Energy Letters, 2020, 5 (12), pp.3837-3842. 10.1021/acsenergylett.0c02002 . hal-03100365

**HAL Id: hal-03100365**

**<https://hal.science/hal-03100365v1>**

Submitted on 18 Oct 2022

**HAL** is a multi-disciplinary open access archive for the deposit and dissemination of scientific research documents, whether they are published or not. The documents may come from teaching and research institutions in France or abroad, or from public or private research centers.

L'archive ouverte pluridisciplinaire **HAL**, est destinée au dépôt et à la diffusion de documents scientifiques de niveau recherche, publiés ou non, émanant des établissements d'enseignement et de recherche français ou étrangers, des laboratoires publics ou privés.

# Repurposing a Bio-Inspired NiFe Hydrogenase Model for CO<sub>2</sub> Reduction with Selective Production of Methane as the Unique C-based Product

Md Estak Ahmed,<sup>a</sup> Suzanne Adam,<sup>b,c</sup> Dibyajyoti Saha,<sup>a</sup> Jennifer Fize,<sup>c</sup> Vincent Artero,<sup>c</sup> Abhishek Dey<sup>a</sup> and Carole Duboc<sup>b</sup>

<sup>a</sup> School of Chemical Sciences, Indian Association for the Cultivation of Science, 2A & 2B Raja S.C. Mullick Road, 700032 Kolkata (India)

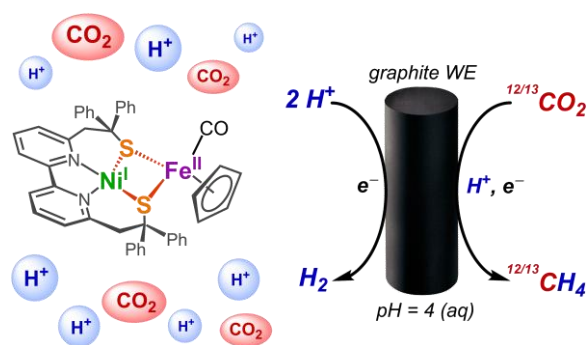
<sup>b</sup> Univ Grenoble Alpes, CNRS, DCM, 38000 Grenoble (France)

<sup>c</sup> Univ Grenoble Alpes, CNRS, CEA, IRIG, Laboratoire de Chimie et Biologie des Métaux, 38000 Grenoble (France)

## Abstract

In the current environmental and economical context, there is an urgent need to conceive catalytic systems to efficiently activate and transform abundant small molecules while demonstrating selectivity when multielectron processes are involved. This is especially true for catalytic production of CH<sub>4</sub> from CO<sub>2</sub>, as a limited number of active photo- or electro-catalysts have been described so far. Herein, we report the unprecedented reactivity of a molecular electrocatalyst physisorbed on a graphite electrode: the bioinspired [L<sup>N2S2</sup>Ni<sup>I</sup>Fe<sup>II</sup>Cp(CO)]<sup>+</sup> (L<sup>N2S2</sup> = 2,2'-(2,2'-bipyridine-6,6'-diyl)bis(1,1'-diphenylethanethiolate) complex selectively and catalytically reduces CO<sub>2</sub> in acidic aqueous solution to produce a mixture of CH<sub>4</sub> and H<sub>2</sub>. Under optimized conditions, at pH 4, faradaic yields of 12% and 66% for CH<sub>4</sub> and H<sub>2</sub> production (TOF<sub>CH<sub>4</sub></sub> = 214 s<sup>-1</sup>, TOF<sub>H<sub>2</sub></sub> ~5.1×10<sup>3</sup> s<sup>-1</sup>), are measured, respectively. We demonstrate that this binuclear NiFe catalyst is stable for hours under controlled potential electrolysis conditions.

## Table of Contents



## **Main text**

The exponential increase in energy demand with an overwhelming dependence on fossil fuels leads to an uncontrolled growth in the CO<sub>2</sub> concentration in the atmosphere. Although CO<sub>2</sub> is the greenhouse gas that contributes most to global warming, it also represents a potential feedstock for the synthesis of value-added fine chemicals and fuels thanks to its high abundance and low cost.<sup>1</sup> However, chemical conversions of CO<sub>2</sub> are difficult because of its high kinetic inertness. Consequently, the development of efficient, and stable catalysts for CO<sub>2</sub> reduction remains one of the key challenges in the energy conversion domain, especially when multielectron processes involving more than two electrons are involved.<sup>2</sup> In this context, selectivity becomes another crucial parameter, since diverse products can be generated as a function of the number of electrons implicated during the reduction process.

Homogeneous CO<sub>2</sub> reduction electrocatalysts have so far demonstrated selectivity for the production of either CO or formate in aprotic solvents. Based on structure/function and mechanistic investigations carried out on series of first-row transition metal catalysts, including polypyridinyl Mn and N-based macrocyclic Fe and Co complexes, rational design of selective and efficient catalytic systems has become possible.<sup>3-11</sup> Their implementation in future devices now requires improving their stability and transitioning to aqueous solution. A promising strategy, developed by several groups, relies on surface immobilization to take full advantage of the benefits of heterogeneous catalysis. Overall, this approach has already demonstrated a considerable improvement to the stability of the electrocatalysts, and the modified electrodes can work in aqueous conditions at various pHs.<sup>12-21</sup>

Intriguingly, in Nature, two enzymes with active sites displaying key structural analogies can either produce H<sub>2</sub> or reduce CO<sub>2</sub>; both contain a heterobinuclear FeNi complex with sulfur-rich coordination spheres (Figure 1). While the [NiFe] hydrogenase generates H<sub>2</sub> from the reversible reduction of H<sup>+</sup>,<sup>22</sup> the CO dehydrogenase reversibly reduces CO<sub>2</sub> to CO.<sup>23-24</sup> Recently, we have reported an electrocatalytic system based on a NiFe model of the [NiFe] hydrogenase, [L<sup>N2S2</sup>Ni<sup>II</sup>Fe<sup>II</sup>Cp(CO)]<sup>+</sup> (L<sup>N2S2</sup> = 2,2'-(2,2'-bipyridine-6,6'-diyl)bis(1,1'-diphenylethanethiolate), named **NiFeCp** (Figure 1, right) physisorbed on a graphite electrode, active in acidic aqueous solutions for H<sub>2</sub> production and robust for hours.<sup>25</sup> In this context, the capability of the same modified edge-plane graphite (EPG) electrode to reduce CO<sub>2</sub> was evaluated. Remarkably, we found that this electrocatalytic system can activate CO<sub>2</sub> and selectively generate CH<sub>4</sub>, as the unique carbon-based product. Production of H<sub>2</sub> is still observed, and under optimal conditions, faradic yields (FY) of 70 and 13 % for H<sub>2</sub> and CH<sub>4</sub> production can be obtained, respectively. We have thus developed a molecular complex modeling common structural features of both the [NiFe] hydrogenase and the CO dehydrogenase, which functions as part of a unique electrocatalytic system that, in the presence of CO<sub>2</sub> and protons, can generate a mixture containing only H<sub>2</sub> and CH<sub>4</sub>.

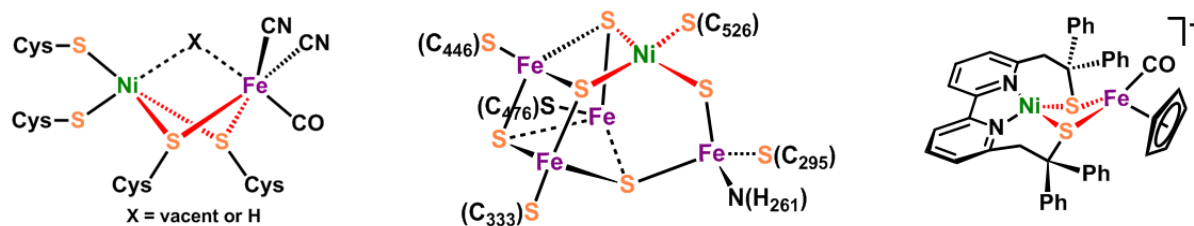


**Figure 1.** Active site structures of [NiFe] hydrogenase (left) and Ni-CODH (middle), and the chemical structure of **NiFeCp** (right).

Modified electrodes have been prepared by physisorption by dropcasting a dichloromethane solution of the binuclear **NiFeCp** complex on EPG electrodes. A previous investigation based on X-ray photoelectron (XPS) and attenuated total reflectance Fourier-transform infrared (ATR-FTIR) spectroscopic data performed on these electrodes, demonstrated that the structure of the heterobinuclear complex is preserved after physisorption.<sup>25</sup> The cyclic voltammogram (CV) of the modified electrode in a 100 mM KPF<sub>6</sub> aqueous solution (pH 5.5) displays an irreversible cathodic signal (mid-wave potential at -0.75 V vs. SHE), assigned to the reduction of [LNi<sup>II</sup>Fe<sup>II</sup>Cp]<sup>+</sup> to [LNi<sup>I</sup>Fe<sup>II</sup>Cp] and an irreversible anodic process ( $E_{pa} = 0.45$  V vs. SHE;  $E_{pc} = 0.18$  V vs. SHE) attributed to the one-electron oxidation of [LNi<sup>II</sup>Fe<sup>II</sup>Cp]<sup>+</sup> (Figure S1). The catalyst surface loading was determined to be  $6 \times 10^{-12}$  mol·cm<sup>-2</sup>.<sup>25</sup>

When the pH value is dropped to 4, the cathodic wave becomes catalytic in nature, this process corresponding to hydrogen evolution (HER).<sup>25</sup> Interestingly, when the same solution is saturated with CO<sub>2</sub> ([CO<sub>2</sub>] ~3.9 mM), the catalytic wave displays a clear 150 mV anodic shift indicative of the fact that a new electrocatalytic process occurs (Figure 2).

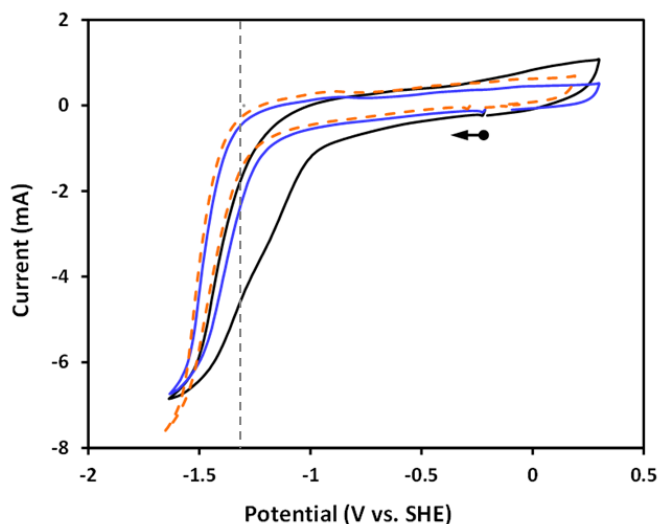


**Figure 2.** CVs of **NiFeCp**-modified EPG electrodes (3.5 mm diameter) in aqueous (pH = 4, phosphate buffer 0.1 M) 100 mM KPF<sub>6</sub> electrolyte at 50 mVs<sup>-1</sup> under either Ar (blue line) or CO<sub>2</sub> (black line) with an Ag/AgCl (satd. KCl) reference and Pt counter electrodes. CV

of pristine EPG electrode (3.5 mm diameter) in aqueous (pH = 4, phosphate buffer 0.1 M) 100 mM KPF<sub>6</sub> electrolyte at 50 mVs<sup>-1</sup> under CO<sub>2</sub> (dashed orange).

Controlled potential electrolysis (CPE) has been carried out at -1.3 V vs. SHE at pH 4 to identify the products. The headspace gas of the CPE cell was then analyzed by gas chromatography (GC). Only two products, H<sub>2</sub> and CH<sub>4</sub>, were detected with a H<sub>2</sub>/CH<sub>4</sub> molar ratio of 23:1 (Table 1, entry 1); the corresponding FY for CH<sub>4</sub> evolution is 12%. No other gaseous product is formed, and analysis of the liquid phase failed to detect methanol or formaldehyde by <sup>1</sup>H NMR, or formate by ion chromatography. In the absence of CO<sub>2</sub> or when unmodified EPG electrodes are used, no CH<sub>4</sub> is generated (Table 1, entry 2).

CPE experiments conducted in the presence of various partial pressures of CO<sub>2</sub> show that the CH<sub>4</sub> production increases linearly as a function of the square root of the concentration of CO<sub>2</sub> (Figure S4), consistent with the fact that CH<sub>4</sub> originates from CO<sub>2</sub>. The H<sub>2</sub>/CH<sub>4</sub> ratio is slightly affected, with a larger production of H<sub>2</sub>, when the CO<sub>2</sub> partial pressure decreases (Table 1, entry 1, and Table S1, entry 1). This ratio is also sensitive to the pH at which the CPE is run (Table 1, entries 1, 6-7). While a ratio of 23:1 is obtained at pH 4, it rises notably when the pH is either increased or decreased, i.e., the H<sub>2</sub>/CH<sub>4</sub> ratios are 30:1 and 50:1 at pH 5 and 3, respectively (Figure S2). This ratio is also slightly affected by the applied potential of the CPE, but to a lesser extent (Table 1, entries 1, 8-10). It remains around 20:1 in the range -0.8 V to -1.3 V vs. SHE and starts to increase at more negative potential (H<sub>2</sub>/CH<sub>4</sub> ratio of 28:1 at -1.4 V vs. SHE) (Figure S3).

**Table 1.** Faradic yields and H<sub>2</sub>/CH<sub>4</sub> ratio as a function of the experimental conditions in CO<sub>2</sub> saturated aqueous buffer.

entry	Catalyst	Applied potential (vs. SHE)	pH	Time (h)	H <sub>2</sub> /CH <sub>4</sub> ratio	Faradic yield (H <sub>2</sub> )	Faradic yield (CH <sub>4</sub> )
1	<b>NiFeCp</b> -EPG	-1.3	4	3	23	62	11
2	EPG	-1.3	4	3	only H <sub>2</sub>	46	N/A
3	Ni-EPG <sup>a</sup>	-1.3	4	3	only H <sub>2</sub>	36	N/A
4	Fe-EPG <sup>b</sup>	-1.3	4	3	only H <sub>2</sub> <sup>c</sup>	35	N/A
5	(S4)NiFeCp-EPG <sup>d</sup>	-1.3	4	3	only H <sub>2</sub> <sup>c</sup>	34	N/A
6	<b>NiFeCp</b> -EPG	-1.3	3	3	50	62	6
7	<b>NiFeCp</b> -EPG	-1.3	5	3	30	64	8
8	<b>NiFeCp</b> -EPG	-0.8	4	3	19	64	13
9	<b>NiFeCp</b> -EPG	<b>-1.0</b>	<b>4</b>	<b>3</b>	<b>22</b>	<b>66</b>	<b>12</b>
10	<b>NiFeCp</b> -EPG	-1.4	4	3	28	61	8

<sup>a)</sup> [NiL<sup>N2S2</sup>] was immobilized instead of NiFeCp, <sup>b)</sup> [CpFe(CO)(CH<sub>3</sub>CN)<sub>2</sub>]<sup>+</sup> was immobilized instead of NiFeCp, <sup>c)</sup> a negligible amount of CH<sub>4</sub> was detected, which was below the quantification limit. <sup>d)</sup> a NiFeCp complex with

a different N2S2 ligand was used:  $[(xbsms)Ni^{II}Fe^{II}Cp(CO)]^+$ ,  $H_2xbsms = 1,2\text{-bis}(4\text{-mercapto-}3,3\text{-dimethyl-}2\text{-thiabutyl)benzene}$ .<sup>26</sup>

CPE run at -1.3 V vs. SHE in pH 4 phosphate buffer 0.1 M displays constant catalytic current at a value of  $\sim 9 \text{ mA/cm}^2$  (Figure S5), with a relatively constant  $H_2/CH_4$  ratio during the first few hours. (Figure S6). The increase of the  $H_2/CH_4$  ratio observed during a 6-hour experiment could be related to the slight increase in pH that was measured after 3 hours (0.3 pH unit). After a CPE experiment carried out under the reference conditions (Table 1, entry 9), faradaic yields of 12% and 66% for  $CH_4$  and  $H_2$ , respectively, were measured (current density at -1.3 V vs. SHE with  $CO_2 = 8.8 \text{ mA}\cdot\text{cm}^{-2}$ , and current density at -1.3 V vs. SHE with Ar =  $0.95 \text{ mA}\cdot\text{cm}^{-2}$ ). After  $\sim 1650\text{s}$  of CPE,  $TON_{CH_4} \sim 3.5 \times 10^5$  and  $TON_{H_2} \sim 8.2 \times 10^6$ ;  $TOF_{CH_4} = 214 \text{ s}^{-1}$ ,  $TOF_{H_2} \sim 5.1 \times 10^3 \text{ s}^{-1}$ ; see SI for detailed calculations, Figure S7).

Gas chromatography coupled to mass spectrometry analysis (GC-MS) confirms that methane is generated during the electrolysis ( $m/z = 16$  with expected mass profile). Interestingly, isotope-labeling experiments were performed with  $^{13}CO_2$  that confirmed that  $^{13}CH_4$  methane ( $m/z = 17$  with expected mass profile) arises from  $CO_2$  reduction (Figure 3).

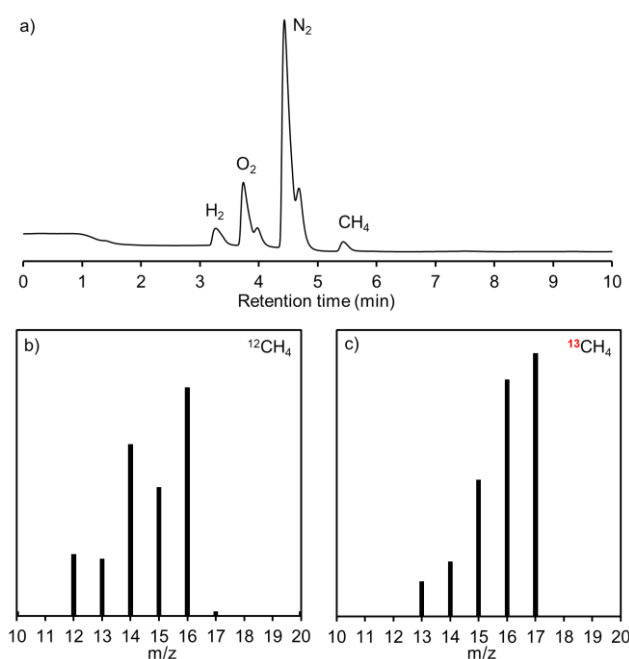


**Figure 3.** GC-MS analysis of the gaseous headspace in the cell following CPE. The gas chromatogram (a), and the mass spectra of the methane product for solutions pre-saturated with  $^{12}CO_2$  or  $^{13}CO_2$  showing  $^{12}CH_4$  (b) and  $^{13}CH_4$  (c). The  $^{13}CH_4$  mass spectrum has been corrected to eliminate water vapor contaminant, based on the NIST spectral database ( $m/z(H_2O) = 18, 17$ ) (See SI for details).

The stable electrolysis current combined with a quasi-constant  $\text{H}_2/\text{CH}_4$  ratio suggests that the **NiFeCp** catalyst is stable under CPE conditions. To provide additional support that the molecular nature of **NiFeCp** is retained during catalysis under such highly acidic conditions, XPS and ATR-FTIR experiments were performed on the modified EPG electrodes before and after electrolysis. The ATR-FTIR spectra are similar (Figure 4, left), both displaying a single CO ligand vibration at  $\bar{\nu}_{\text{CO}} = 1916 \text{ cm}^{-1}$ , previously assigned to the Fe-bound CO in immobilized **NiFeCp** ( $1926 \text{ cm}^{-1}$  in an ATR-IR spectrum of the powder sample of **NiFeCp**).<sup>25</sup> Additionally, both XPS spectra recorded before and after electrolysis are characterized by a single peak at  $854.4 \text{ eV}$  in the Ni 2p core region (Figure 5, top), which was previously unambiguously assigned to **NiFeCp**.<sup>25</sup> In the same vein, the two XPS spectra recorded in the Fe 2p core region display a similar single peak at  $708.9 \text{ eV}$ , in agreement with the presence of a single Fe-based species (Figure 5, bottom). Finally, the CVs of the modified EPG electrode recorded before and after a CPE experiment under the reference conditions are comparable, indicating that the adsorbed complex still displays the redox properties of the molecular **NiFeCp** complex (Figure 4, right). The small current shift between the two CVs can be explained by the modification of the pH occurring during the CPE experiment.

We have also tested another known binuclear NiFe HER electrocatalyst,  $[(\text{xbsms})\text{Ni}^{\text{II}}\text{Fe}^{\text{II}}\text{Cp}(\text{CO})]^+$ ,<sup>26</sup> which also contains a NiFeS<sub>2</sub> core, but the Ni ion is in a S<sub>4</sub> environment instead of an N<sub>2</sub>S<sub>2</sub> one, as in **NiFeCp**. Interestingly, the corresponding modified EPG electrode displays only HER catalytic activity, but no product arising from CO<sub>2</sub> reduction is generated (Table 1, entry 5). Taken together, these experiments confirm that the reactivity of **NiFeCp** is specific to its molecular structure, which is entirely retained after electrolysis when immobilized onto an EPG electrode.

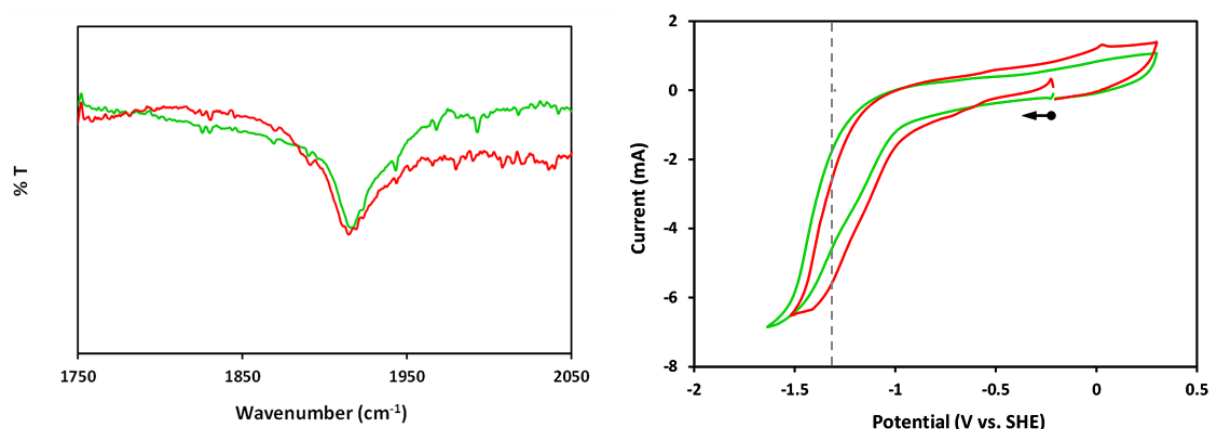


**Figure 4.** ATR-FTIR spectra (left) and CVs (right) of electrodes drop-cast with  $[\text{LNi}^{\text{II}}\text{Fe}^{\text{II}}\text{Cp}]^+$  as prepared (green traces) and after 2 h electrolysis at  $-1.3 \text{ V vs. SHE}$  (red traces), in degassed pH 4 phosphate buffer 0.1 M with 100 mM  $\text{KPF}_6$  electrolyte.

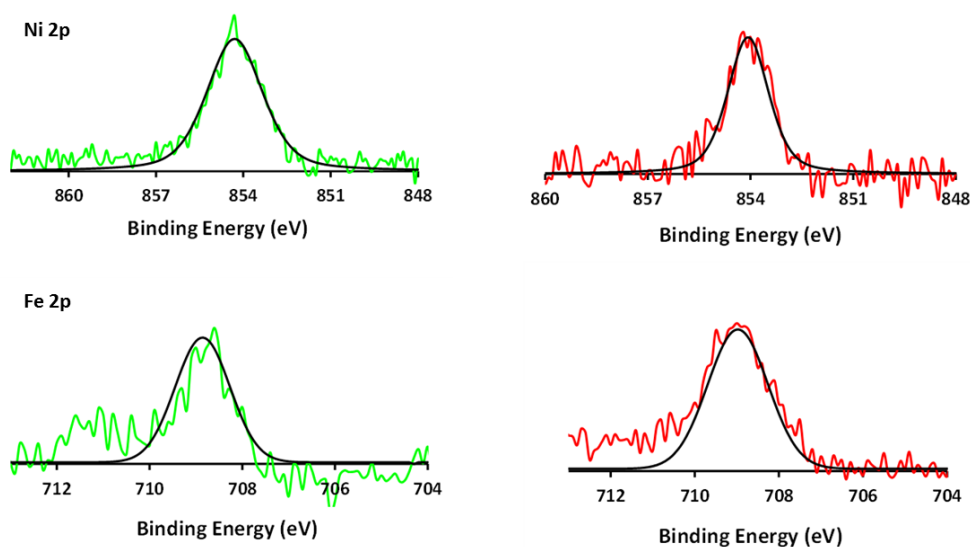


**Figure 5.** XPS spectra at the Ni 2p and Fe 2p core level of electrodes drop-cast with  $[\text{LNi}^{\text{II}}\text{Fe}^{\text{II}}\text{Cp}]^+$  as prepared (left) and after 2 h electrolysis at -1.3 V vs. SHE in degassed pH 4 phosphate buffer with 100 mM  $\text{KPF}_6$  electrolyte (right).

The molecular catalyst described here distinguishes itself from almost all known systems by producing  $\text{CH}_4$  as the only carbon-based product, rather than mixtures of CO, short chain alkanes, and/or  $\text{HCOOH}$ . In the literature, the number of reported catalytic systems capable of generating products such as long-chain ( $\text{C}_2+$ ) alkanes<sup>27-28</sup> or alcohols<sup>18, 29</sup> is limited, and they generally display modest efficiency. In the specific case of  $\text{CH}_4$  production, only two main families of catalysts have been described based on two different approaches: (i) molecular metal-based porphyrins and derivatives either via photocatalytic processes in aprotic solvents or via electrocatalysis in aqueous solutions when immobilized on modified electrodes,<sup>20-21, 30-32</sup> and (ii) metallic Cu-based materials working in aqueous solution.<sup>33-39</sup> In general, the electrochemical production of methane from aqueous  $\text{CO}_2$  is observed for overpotential values higher than 0.8 V.<sup>40-41</sup> Physically adsorbed **NiFeCp** mediates  $\text{CH}_4$  evolution (apparent standard potential is 0.17 V vs. the Reversible Hydrogen Electrode) from -0.8 V vs. SHE in pH 4 aqueous buffer, corresponding to  $\sim 0.75$  V onset overpotential requirement. At the mid-wave potential (-1.2 V vs. SHE) of the catalytic wave (Figure 2), for a more accurate description of the performance of a molecular electrocatalyst,<sup>42</sup> the overpotential for  $\text{CH}_4$  evolution is 1.13 V. Our molecular catalyst thus compares well with previously reported heterogeneous catalysts including immobilized molecular complexes.<sup>20, 32</sup>

Electrochemical methane production on metallic (M) surfaces generally involves a M-CO intermediate,<sup>43-45</sup> although such an intermediate can be overcome for single-atom catalysts.<sup>46</sup> In the case of physically adsorbed **NiFeCp**,  $\text{CO}_2$  reduction is inhibited in the presence of external CO, and only hydrogen is detected as the product (Table S1, entry 2). These observations indicate that CO is not involved as an intermediate during the  $\text{CO}_2$  reduction process. Based on experimental data and DFT calculations, it has been



previously proposed that under homogeneous conditions, CO terminally binds at the Fe site of the reduced [LNi<sup>I</sup>Fe<sup>II</sup>Cp] complex.<sup>47</sup> However, the electrocatalyst remains active for H<sub>2</sub> production, though to a lesser extent, with hydride species being generated at the Ni site.<sup>48-49</sup> We can thus propose that a similar process takes place here, with CO blocking the Fe site, preventing the CO<sub>2</sub> activation, but leaving the Ni site available for HER activity.

Overall our data suggest that production of CH<sub>4</sub> proceeds through a mechanism involving two sites acting in a concerted manner, where CO<sub>2</sub> is activated and transformed at one metal site, while the second metal site delivers hydride to the first site until CH<sub>4</sub> is formed and released. Similar mechanisms have been proposed with Cu-based electrodes,<sup>44</sup> and also for bimetallic nanoalloy catalysts, in which each metal plays a distinct role: one to activate the C-based intermediate products, and the second to stabilize the hydride species.<sup>34</sup>

The selectivity of this present molecular catalyst, which can go beyond a 2-electron CO<sub>2</sub> reduction process, is unique even when compared with the best metal-based materials described so far. Further studies are in progress in our laboratories to decipher the unique reaction mechanism underlying such a behavior. In parallel, ligand design is underway to tune the reactivity of physisorbed **NiFeCp** complexes and increase the selectivity for CH<sub>4</sub> production over proton reduction.

**Supporting Information Available:** Experimental methods (preparation of the modified electrodes, description of the spectroscopic techniques and of the electrochemical techniques), additional data (redox properties of the modified electrodes, catalytic performance under different experimental conditions).

**Acknowledgments.** Financial support for this work was provided by the Agence National de la Recherche in the framework of the “Investissements d’avenir” Program (ANR- 15-IDEX-02), the Labex ARCANE (ANR-11-LABX-003), and the CBH-EUR-GS(ANR-17-EURE-0003), and ANR-DFG (ANR-16-CE92\_0012\_01 NiFeMim), the Indo-French Center for the Promotion of Advanced Research (IFCPAR/CEFIPRA grant no 5405-1).

## References

1. Lim, X., How to make the most of carbon dioxide. *Nature* **2016**, *526*, 628-630.
2. Francke, R.; Schille, B.; Roemelt, M., Homogeneously Catalyzed Electroreduction of Carbon Dioxide—Methods, Mechanisms, and Catalysts. *Chem. Rev.* **2018**, *118*, 4631-4701.
3. Ahmed, M. E.; Rana, A.; Saha, R.; Dey, S.; Dey, A., Homogeneous Electrochemical Reduction of CO<sub>2</sub> to CO by a Cobalt Pyridine Thiolate Complex. *Inorg. Chem.* **2020**, *59*, 5292-5302.
4. Rønne, M. H.; Cho, D.; Madsen, M. R.; Jakobsen, J. B.; Eom, S.; Escoudé, É.; Hammershøj, H. C. D.; Nielsen, D. U.; Pedersen, S. U.; Baik, M.-H.; Skrydstrup, T.; Daasbjerg, K., Ligand-Controlled Product Selectivity in Electrochemical Carbon Dioxide Reduction Using Manganese Bipyridine Catalysts. *J. Am. Chem. Soc.* **2020**, *142*, 4265-4275.

5. Liu, D.-C.; Zhong, D.-C.; Lu, T.-B., Non-noble metal-based molecular complexes for CO<sub>2</sub> reduction: From the ligand design perspective. *EnergyChem* **2020**, *2*, 100034.
6. Margarit, C. G.; Asimow, N. G.; Costentin, C.; Nocera, D. G., Tertiary Amine-Assisted Electroreduction of Carbon Dioxide to Formate Catalyzed by Iron Tetraphenylporphyrin. *ACS Energy Lett.* **2020**, *5*, 72-78.
7. Fokin, I.; Denisiuk, A.; Würtele, C.; Siewert, I., The Impact of a Proton Relay in Binuclear  $\alpha$ -Diimine-Mn(CO)<sub>3</sub> Complexes on the CO<sub>2</sub> Reduction Catalysis. *Inorg. Chem.* **2019**, *58*, 10444-10453.
8. Gotico, P.; Halime, Z.; Aukauloo, A., Recent advances in metalloporphyrin-based catalyst design towards carbon dioxide reduction: from bio-inspired second coordination sphere modifications to hierarchical architectures. *Dalton Trans.* **2020**, *49*, 2381-2396.
9. Franco, F.; Fernández, S.; Lloret-Fillol, J., Advances in the electrochemical catalytic reduction of CO<sub>2</sub> with metal complexes. *Curr. Opin. Electrochem.* **2019**, *15*, 109-117.
10. Fukuzumi, S.; Lee, Y.-M.; Ahn, H. S.; Nam, W., Mechanisms of catalytic reduction of CO<sub>2</sub> with heme and nonheme metal complexes. *Chem. Sci.* **2018**, *9*, 6017-6034.
11. Queyriaux, N.; Abel, K.; Fize, J.; Pécaut, J.; Orio, M.; Hammarström, L., From non-innocent to guilty: on the role of redox-active ligands in the electro-assisted reduction of CO<sub>2</sub> mediated by a cobalt(ii)-polypyridyl complex. *Sustain. Energy Fuels* **2020**, *4*, 3668-3676.
12. Abdinejad, M.; Dao, C.; Deng, B.; Dinic, F.; Voznyy, O.; Zhang, X.-a.; Kraatz, H.-B., Electrocatalytic Reduction of CO<sub>2</sub> to CH<sub>4</sub> and CO in Aqueous Solution Using Pyridine-Porphyrins Immobilized onto Carbon Nanotubes. *ACS Sustain. Chem. Eng.* **2020**, *8*, 9549-9557.
13. Torbensen, K.; Boudy, B.; Joulié, D.; von Wolff, N.; Robert, M., Emergence of CO<sub>2</sub> electrolyzers including supported molecular catalysts. *Curr. Opin. Electrochem.* **2020**, *24*, 49-55.
14. Zhang, S.; Fan, Q.; Xia, R.; Meyer, T. J., CO<sub>2</sub> Reduction: From Homogeneous to Heterogeneous Electrocatalysis. *Acc. Chem. Res.* **2020**, *53*, 255-264.
15. Sun, L.; Reddu, V.; Fisher, A. C.; Wang, X., Electrocatalytic reduction of carbon dioxide: opportunities with heterogeneous molecular catalysts. *Energy Environ. Sci.* **2020**, *13*, 374-403.
16. Ren, S.; Joulié, D.; Salvatore, D.; Torbensen, K.; Wang, M.; Robert, M.; Berlinguette, C. P., Molecular electrocatalysts can mediate fast, selective CO<sub>2</sub> reduction in a flow cell. *Science* **2019**, *365*, 367.
17. Wang, M.; Chen, L.; Lau, T.-C.; Robert, M., A Hybrid Co Quaterpyridine Complex/Carbon Nanotube Catalytic Material for CO<sub>2</sub> Reduction in Water. *Angew. Chem. Int. Ed.* **2018**, *57*, 7769-7773.
18. Wu, Y.; Jiang, Z.; Lu, X.; Liang, Y.; Wang, H., Domino electroreduction of CO<sub>2</sub> to methanol on a molecular catalyst. *Nature* **2019**, *575*, 639-642.
19. Wang, M.; Torbensen, K.; Salvatore, D.; Ren, S.; Joulié, D.; Dumoulin, F.; Mendoza, D.; Lassalle-Kaiser, B.; Işci, U.; Berlinguette, C. P.; Robert, M., CO<sub>2</sub> electrochemical catalytic reduction with a highly active cobalt phthalocyanine. *Nat. Commun.* **2019**, *10*, 3602.
20. Weng, Z.; Wu, Y.; Wang, M.; Jiang, J.; Yang, K.; Huo, S.; Wang, X.-F.; Ma, Q.; Brudvig, G. W.; Batista, V. S.; Liang, Y.; Feng, Z.; Wang, H., Active sites of copper-complex catalytic materials for electrochemical carbon dioxide reduction. *Nat. Commun.* **2018**, *9*, 415.
21. Weng, Z.; Jiang, J.; Wu, Y.; Wu, Z.; Guo, X.; Materna, K. L.; Liu, W.; Batista, V. S.; Brudvig, G. W.; Wang, H., Electrochemical CO<sub>2</sub> Reduction to Hydrocarbons on a

Heterogeneous Molecular Cu Catalyst in Aqueous Solution. *J. Am. Chem. Soc.* **2016**, *138*, 8076-8079.

22. Lubitz, W.; Ogata, H.; Rüdiger, O.; Reijerse, E., Hydrogenases. *Chem. Rev.* **2014**, *114*, 4081-4148.

23. Can, M.; Armstrong, F. A.; Ragsdale, S. W., Structure, Function, and Mechanism of the Nickel Metalloenzymes, CO Dehydrogenase, and Acetyl-CoA Synthase. *Chem. Rev.* **2014**, *114*, 4149-4174.

24. Appel, A. M.; Bercaw, J. E.; Bocarsly, A. B.; Dobbek, H.; DuBois, D. L.; Dupuis, M.; Ferry, J. G.; Fujita, E.; Hille, R.; Kenis, P. J. A.; Kerfeld, C. A.; Morris, R. H.; Peden, C. H. F.; Portis, A. R.; Ragsdale, S. W.; Rauchfuss, T. B.; Reek, J. N. H.; Seefeldt, L. C.; Thauer, R. K.; Waldrop, G. L., Frontiers, Opportunities, and Challenges in Biochemical and Chemical Catalysis of CO<sub>2</sub> Fixation. *Chem. rev.* **2013**, *113*, 6621-6658.

25. Ahmed, M. E.; Chattopadhyay, S.; Wang, L. K.; Brazzolotto, D.; Pramanik, D.; Aldakov, D.; Fize, J.; Morozan, A.; Gennari, M.; Duboc, C.; Dey, A.; Artero, V., Hydrogen Evolution from Aqueous Solutions Mediated by a Heterogenized NiFe -Hydrogenase Model: Low pH Enables Catalysis through an Enzyme-Relevant Mechanism. *Angew. Chem. Int. Ed.* **2018**, *57*, 16001-16004.

26. Canaguier, S.; Field, M.; Oudart, Y.; Pecaut, J.; Fontecave, M.; Artero, V., A structural and functional mimic of the active site of NiFe hydrogenases. *Chem. Commun.* **2010**, *46*, 5876-5878.

27. Centi, G.; Perathoner, S.; Winè, G.; Gangeri, M., Electrocatalytic conversion of CO<sub>2</sub> to long carbon-chain hydrocarbons. *Green Chem.* **2007**, *9*, 671-678.

28. Vasileff, A.; Zhu, Y.; Zhi, X.; Zhao, Y.; Ge, L.; Chen, H. M.; Zheng, Y.; Qiao, S.-Z., Electrochemical Reduction of CO<sub>2</sub> to Ethane through Stabilization of an Ethoxy Intermediate. *Angew. Chem. Int. Ed.* **2020**, *59*, 19649-19653.

29. Liu, Y.; Li, F.; Zhang, X.; Ji, X., Recent progress on electrochemical reduction of CO<sub>2</sub> to methanol. *Curr. Opin. Green Sustain. Chem.* **2020**, *23*, 10-17.

30. Rao, H.; Schmidt, L. C.; Bonin, J.; Robert, M., Visible-light-driven methane formation from CO<sub>2</sub> with a molecular iron catalyst. *Nature* **2017**, *548*, 74.

31. Rao, H.; Lim, C.-H.; Bonin, J.; Miyake, G. M.; Robert, M., Visible-Light-Driven Conversion of CO<sub>2</sub> to CH<sub>4</sub> with an Organic Sensitizer and an Iron Porphyrin Catalyst. *J. Am. Chem. Soc.* **2018**, *140*, 17830-17834.

32. Shen, J.; Kortlever, R.; Kas, R.; Birdja, Y. Y.; Diaz-Morales, O.; Kwon, Y.; Ledezma-Yanez, I.; Schouten, K. J. P.; Mul, G.; Koper, M. T. M., Electrocatalytic reduction of carbon dioxide to carbon monoxide and methane at an immobilized cobalt protoporphyrin. *Nat. Commun.* **2015**, *6*, 8177.

33. Kuhl, K. P.; Cave, E. R.; Abram, D. N.; Jaramillo, T. F., New insights into the electrochemical reduction of carbon dioxide on metallic copper surfaces. *Energy Environ. Sci.* **2012**, *5*, 7050-7059.

34. Zhang, S.; Kang, P.; Bakir, M.; Lapides, A. M.; Dares, C. J.; Meyer, T. J., Polymer-supported CuPd nanoalloy as a synergistic catalyst for electrocatalytic reduction of carbon dioxide to methane. *Proc. Natl. Acad. Sci. U.S.A.* **2015**, *112*, 15809-15814.

35. Varela, A. S.; Ju, W.; Reier, T.; Strasser, P., Tuning the Catalytic Activity and Selectivity of Cu for CO<sub>2</sub> Electroreduction in the Presence of Halides. *ACS Catal.* **2016**, *6*, 2136-2144.

36. Pérez-Gallent, E.; Marcandalli, G.; Figueiredo, M. C.; Calle-Vallejo, F.; Koper, M. T. M., Structure- and Potential-Dependent Cation Effects on CO Reduction at Copper Single-Crystal Electrodes. *J. Am. Chem. Soc.* **2017**, *139*, 16412-16419.

37. Kim, J.; Song, J. T.; Ryoo, H.; Kim, J.-G.; Chung, S.-Y.; Oh, J., Morphology-controlled Au nanostructures for efficient and selective electrochemical CO<sub>2</sub> reduction. *J. Mat. Chem. A* **2018**, *6*, 5119-5128.
38. Iyengar, P.; Huang, J.; De Gregorio, G. L.; Gadiyar, C.; Buonsanti, R., Size dependent selectivity of Cu nano-octahedra catalysts for the electrochemical reduction of CO<sub>2</sub> to CH<sub>4</sub>. *Chem. Commun.* **2019**, *55*, 8796-8799.
39. Pan, H.; Barile, C. J., Electrochemical CO<sub>2</sub> reduction to methane with remarkably high Faradaic efficiency in the presence of a proton permeable membrane. *Energy Environ. Sci.* **2020**, *13*, 3567-3578.
40. Larrazábal, G. O.; Martín, A. J.; Pérez-Ramírez, J., Building Blocks for High Performance in Electrocatalytic CO<sub>2</sub> Reduction: Materials, Optimization Strategies, and Device Engineering. *J. Phys. Chem. Lett.* **2017**, *8*, 3933-3944.
41. note, *Pt has been shown to be active for methane evolution with almost no overpotential requirement although with low faradic efficiency and low CO<sub>2</sub> partial pressures, see Umeda et al., ACS Appl. Energy Mater.* **2020**, *3*, 1, 1119-1127.
42. Fourmond, V.; Jacques, P.-A.; Fontecave, M.; Artero, V., H<sub>2</sub> Evolution and Molecular Electrocatalysts: Determination of Overpotentials and Effect of Homoconjugation. *Inorg. Chem.* **2010**, *49*, 10338-10347.
43. Nitopi, S.; Bertheussen, E.; Scott, S. B.; Liu, X.; Engstfeld, A. K.; Horch, S.; Seger, B.; Stephens, I. E. L.; Chan, K.; Hahn, C.; Nørskov, J. K.; Jaramillo, T. F.; Chorkendorff, I., Progress and Perspectives of Electrochemical CO<sub>2</sub> Reduction on Copper in Aqueous Electrolyte. *Chem. Rev.* **2019**, *119*, 7610-7672.
44. Schreier, M.; Yoon, Y.; Jackson, M. N.; Surendranath, Y., Competition between H and CO for Active Sites Governs Copper-Mediated Electrosynthesis of Hydrocarbon Fuels. *Angew. Chem. Int. Ed.* **2018**, *57*, 10221-10225.
45. Kortlever, R.; Shen, J.; Schouten, K. J. P.; Calle-Vallejo, F.; Koper, M. T. M., Catalysts and Reaction Pathways for the Electrochemical Reduction of Carbon Dioxide. *J. Phys. Chem. Lett.* **2015**, *6*, 4073-4082.
46. Han, L.; Song, S.; Liu, M.; Yao, S.; Liang, Z.; Cheng, H.; Ren, Z.; Liu, W.; Lin, R.; Qi, G.; Liu, X.; Wu, Q.; Luo, J.; Xin, H. L., Stable and Efficient Single-Atom Zn Catalyst for CO<sub>2</sub> Reduction to CH<sub>4</sub>. *J. Am. Chem. Soc.* **2020**, *142*, 12563-12567.
47. Brazzolotto, D.; Wang, L. K.; Tang, H.; Gennari, M.; Queyriaux, N.; Philouze, C.; Demeshko, S.; Meyer, F.; Orio, M.; Artero, V.; Hall, M. B.; Duboc, C., Tuning Reactivity of Bioinspired NiFe -Hydrogenase Models by Ligand Design and Modeling the CO Inhibition Process. *ACS Catal.* **2018**, *8*, 10658-10667.
48. Tang, H.; Hall, M. B., Biomimetics of [NiFe]-Hydrogenase: Nickel- or Iron-Centered Proton Reduction Catalysis? *J. Am. Chem. Soc.* **2017**, *139*, 18065-18070.
49. Brazzolotto, D.; Gennari, M.; Queyriaux, N.; Simmons, T. R.; Pécaut, J.; Demeshko, S.; Meyer, F.; Orio, M.; Artero, V.; Duboc, C., Nickel-centred proton reduction catalysis in a model of [NiFe] hydrogenase. *Nat. Chem.* **2016**, *8*, 1054-1060.